420-Gb/s/channel WDM PS-64QAM Transmission Over 4,000-km ULAF Using Ring-Wise Neural Network Equalization

Bohan Sang[1], Miao Kong[1], Wen Zhou[1], Jianyu Long[1], Li Zhao[1], Bing Ye[2], Weizhang Chen[2], Xiangjun Xin[3], Bo Liu[3] and Jianjun Yu[1,*]

[1] *Fudan University, Shanghai, China, 200433*
[2] *ZTE Corp., Beijing, China, 100191*
[3] *Beijing University of Posts and Telecommunications, Beijing, China, 100876*

[*] *jianjun@fudan.edu.cn*

Abstract: We realized 420-Gbit/s/channel WDM coherent transmission over 4,000-km ULAF utilizing a novel well-expandable Ring-Wise Neural Network equalizer (RW-NNE) targeted to PS-64QAM signals. Results show that our RW-NNE with 25.3%-lower complexity outperforms normal NNE by 25% reach improvement.

1. Introduction

Due to the explosive growth of bandwidth requirements for new technologies and new applications, the bit rate improvement of optical communication systems has become an important requirement for the development of human society. Nonlinearities brought by fibers and photoelectric devices have always been a major factor restricting the performance of optical fiber communication systems. Many researches about the nonlinearity compensation have been proposed, including Neural Network Equalization (NNE) [1,2], Volterra Equalization (VE) [3] and digital back propagation (DBP) [4]. Recently, NNE has been proved to be an effective nonlinear compensation (NLC) algorithm in multiple communication scenarios. Due to its strong adaptability and nonlinear representation ability, various types of NNE are continuously used in long-haul transmission systems for nonlinear compensation [5–7]. On the other hand, Probabilistic Shaping (PS) has always been a core technique for achieving a sensitivity gain and approaching Shannon capacity [3,8,9]. By using Constant Composition Distribution Matching (CCDM), the source entropy can be flexibly adjusted and the power can be matched to the optimal MB distribution. However, combining PS and NNE techniques will be a huge challenge. Due to the uneven distribution of PS signals, the performance of NNE is limited under the influence of the imbalanced training set. Inner constellation points (with low amplitudes) obtain additional training relative to the outer constellation points, so the trained weights are useful for equalizing inner points while being very inaccurate for the outer points. Note that it does not mean that the nonlinear representation ability of NN is decreased, but that the weights are not effectively trained due to the imbalance distribution of PS signals.

In our previous published work, we proposed Truncated-PS (TPS) to make the probability distribution of the PS signals more even, and this made it easier for CMA and Volterra-LMS training [3]. Also, we implemented complicated Long Short-Term Memory (LSTM) model to memory NNE data with low probabilities [10]. These solutions can alleviate the mentioned problem but they are not yet perfect, and there is a tradeoff between the optimal QAM power distribution and the balance training.

In this paper, we propose Ring-Wise NNE (RW-NNE) that innovatively divided the training sequence into inner and outer groups according to amplitude information, and different NN models are built for two groups. An overlapping mechanism is proposed to accurately identify the junction points between the inner and outer rings. The proposed RW-NNE is proved in 48-Gbaud PS-64QAM (SE=5.5) WDM transmission system over Raman-amplified ultra-large effective area fiber (ULAF). The results show that RW-NNE extends the transmission distance from 3,200 km to 4,000 km compared to normal NNE.

2. Ring-Wise Neural Network Equalization

Compared with normal NNE, RW-NNE reduces the unevenness of the training data, and make the weights of NNE better trained. Inspired by Ref. [2], , that multi-label binary DNN can gain a performance by dividing complex high-order equalization task into multiple simple binary classification task, we separate inner and outer constellation points according to the amplitude, and build different training models.

Specifically, considering the 9 rings in 64-QAM constellation (see Fig. 1(a)), we designed two NNs for the equalization for inner rings and outer rings, respectively. Fig. 1(b) shows the points distribution of each ring, it can be seen that after dividing the inner and outer training sets, the distribution becomes more balanced for NN. We use ordinary fully-connect NN with two hidden layers in Fig. 1(c) to prove the superiority of ring wise.

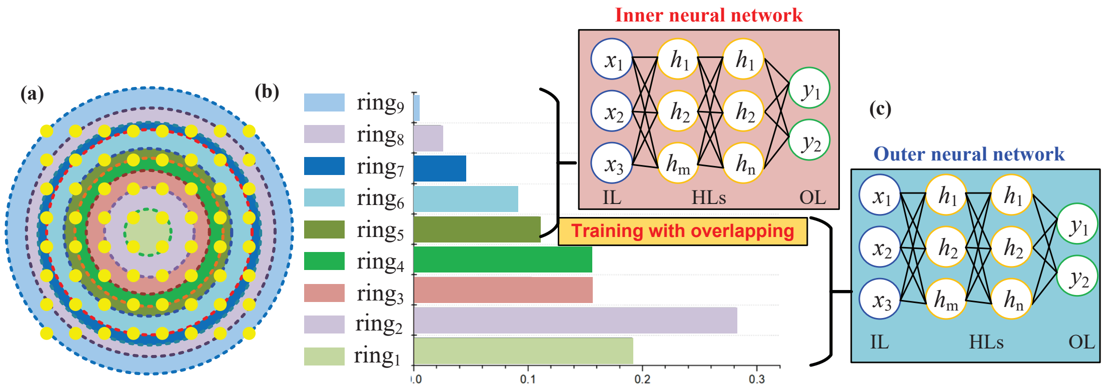

Fig. 1. (a) PS-64QAM constellation in rings; (b) Ring distribution of PS-64QAM signals (SE=5.5); (c) The inner and outer NN in RW-NNE.

In training, the points are separated according to the train labels. These signals can be easily assigned to the training dataset in inner or outer NN. However, it's difficult to determine the received signal to the corresponding ring without errors. By observing and counting the errors of ring decision, we find that after the DSP chain without NLC, there's no misjudgment between the 4th and 6th rings due to the big amplitude gap. Therefore, we set the 5th ring as the overlapping area between the inner and outer NN, which means that the signals at the 5th ring are sent both to the inner NN and the outer NN. In testing, the decision boundary is set right at the 5th ring: the points out of the 5th ring (with amplitudes exceed the radius of the 5th ring) go to the outer NN and those inside the 5th ring go to the inner NN. Both inner and outer NN can handle signals at 5th ring, so the bit errors caused by assigning NNs are avoided. Notice that the training data is the signal block obtained from the sliding window of the received signals. The assignment of inner NN and outer NN doesn't change the training data, the pair of training data and training label is assigned together according to the ring-belonging of the training label. Furthermore, in our proposed RW-NNE, each of the signal only passes through one NN, which means that there's no complexity penalty by replacing normal NNE with RW-NNE. At the same time, because of the equalization simplification, less neurons are needed in hidden layers of each sub-NN in RW-NNE than those in normal NNE. The numerical comparison is given in detail in Sec. 4.

3. Experimental Setup

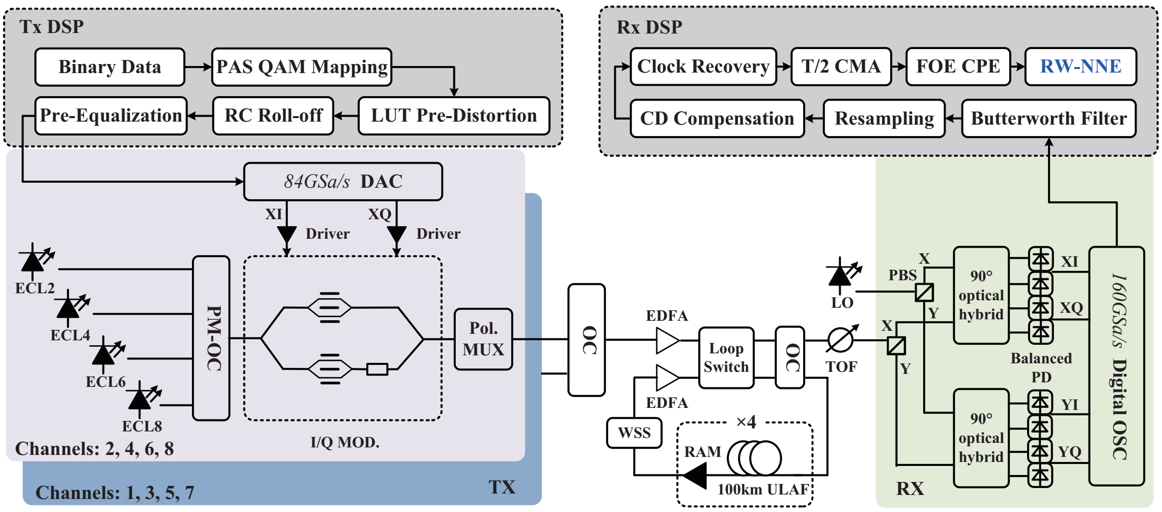

Fig. 2. Experimental Setup and the flowchart of offline DSP at Tx and Rx end.

The transmitter-block consisted of a commercial DAC with 20-GHz analog bandwidth and 84-GSa/s sampling rate, a 100-kHz-linewidth external cavity laser (ECL), a 32-GHz bandwidth I/Q modulator, two 65-GHz modulator drivers and a polarization multiplexer (Pol. MUX). For optical signal modulation, the light source at 1553.126-nm from the ECL was fed into the I/Q modulator driven by the pre-processed signals. After optical modulation, a Pol. MUX was utilized to realize polarization multiplexing. At the transmitter-side, 8-channel 50 GHz-WDM PM signals, which were divided into odd-channel group (Ch. 1, 3, 5 and 7) and even-channel group (Ch. 2, 4, 6 and 8), were combined by a polarization maintaining optical coupler (PM-OC) and launched into the recirculating ULAF loop with backward-pumped Raman amplifier, which consisted of several spans of 400-km TeraWave+ fiber with an average effective area of 125-μm2, an attenuation coefficient of 0.182-dB/km and a chromatic dispersion coefficient of 20-ps/(nm·km) at 1550 nm. In the recirculating loop, a backward-pumped Raman amplifier with 20-dB ON-OFF gain was utilized to compensate for signal loss for each span. The average power of the Raman pumps is around 950-mW. What's more, we used an attenuator (ATT) to control the optical power and a WSS was used to flatten the gain slope of the band-pass filter.

At the receiver end, a tunable optical filter (TOF) with 3-dB bandwidth of 0.9 nm was used to select the desired sub-channel from the 8-channel WDM signals. In our experiment, the 4-th sub-channel is selected by the TOF. Then we implemented the polarization- and phase-diversity operation for the selected WDM signal and the 100-kHz-linewidth optical local oscillator (LO) using two polarization beam splitters (PBSs) and two 90° optical hybrids. Afterwards, the outputs of hybrids were fed into four balanced photodetectors (PDs), each with a bandwidth of 70-GHz. Finally, the digitization and sampling were realized by the digital oscilloscope (OSC) with 65-GHz bandwidth and 160-GSa/s sampling rate, which was followed by the offline DSP. The offline DSP consisted of Butterworth digital low-pass filter, resampling, chromatic dispersion (CD) compensation, clock recovery, T/2 CMA, frequency offset estimation (FOE), carrier-phase-estimation (CPE) based on blind-phasesearch (BPS) and the proposed RW-NNE.

4. Results and Discussion

We tested the system performance both in Back-to-Back (BtB) and ULAF transmission. We compared the proposed RW-NNE with normal NNE and Volterra equalization, and the results are shown in Fig. 3. It can be seen that in BtB case, fiber nonlinearity is not the dominating factor influencing the performance. By using LDPC with 20% overhead in [3], 420-Gb/s transmission can be achieved. The proposed RW-NNE can extend the transmission distance to 4000-km, which is much better than normal NNE and VE. Also, RW-NNE with less hidden neurons (160 & 80) saved 25.3% complexity comparing to normal NNE (200 & 120). The complexity can be further reduced by weight pruning [1, 10], which is beyond the scope of this paper.

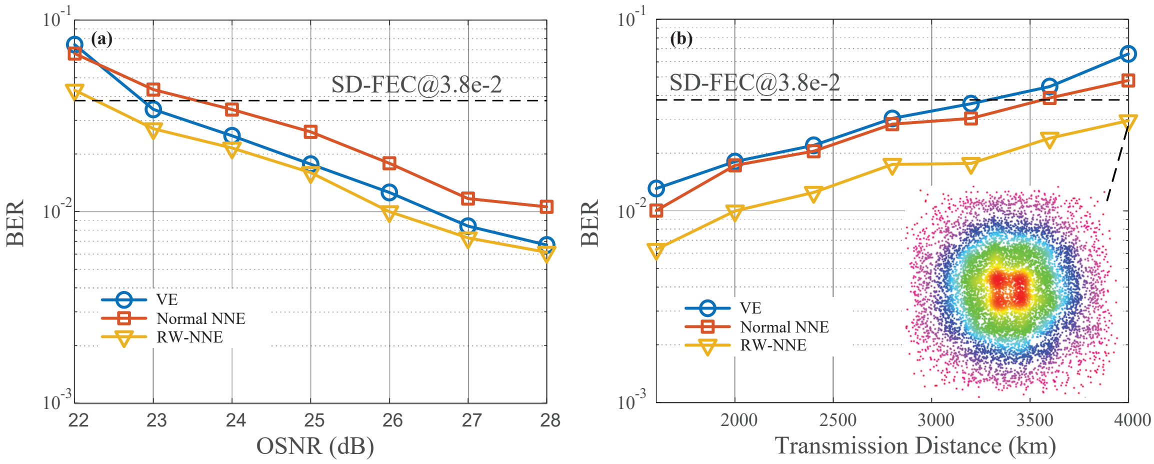

Fig. 3. (a) BER vs. OSNR in BtB case; (b) BER vs. ULAF transmission distance.

5. Conclusions

We successfully realized 420Gb/s/channel PS-64QAM WDM coherent transmission over 4,000-km ULAF utilizing the proposed RW-NNE. Results show that our RW-NNE with 25.3%-lower complexity outperforms normal NNE by 25% reach improvement. Our work is well-expandable, the NN model in RW-NNE can be more advanced and the rings can be divided into more parts with overlapping. *This work is partially supported by the National Key R & D Program of China (2018YFB1801004) and NNSF of China (Grant number 61935005, 61835002).*

References

1. S. Fujisawa et al., OFC, M5F.1, 2021.
2. T. Koike-Akino et al., JLT, vol. 38, no. 11, pp. 3059–3066, 2020.
3. M. Kong et al., JLT, vol. 40, no. 9, pp. 2830–2839, 2022.
4. E. Sillekens et al., SiPS, pp. 1–4, 2020.
5. S. Deligiannidis et al., JLT, vol. 38, no. 21, pp. 5991–5999, 2020.
6. O. Sidelnikov et al., CLEO/Europe-EQEC, pp. 1–1, 2021.
7. K. Peng et al., ICOCN, pp. 1–3, 2022.
8. E. Ip et al., JLT, vol. 37, no. 1, pp. 148–155, 2019.
9. F. Roumestan et al., ECOC, pp. 1–4, 2021.
10. B. Sang et al., ECOC, pp. 1–4, 2022.